NGI Teknisk notat

Til:	Norwegian Water Resources and Energy Directorate (NVE)
v/:	Odd Are jensen
Kopi til:	
Dato:	2020-08-28
Rev.nr. / Rev.dato:	0/
Dokumentnr.:	20150457-10-TN
Prosjekt:	Nye aktsomhetskart snøskred
Prosjektleder:	Ulrik Domaas
Utarbeidet av:	Dieter Issler
Kontrollert av:	Kjersti Gisnås

Approaches to Including Climate and Forest Effects in Avalanche Hazard Indication Maps in Norway

Sammendrag / ***Abstract***

The modeling system NAKSIN generates regional avalanche hazard indication maps in a largely automatic manner. Potential release areas are determined by topographic conditions. The corresponding release probabilities and fracture depths are estimated as a function of topographic and climatic factors as well as of forest density and quality. The hazardous area is determined by simulating run-out from each identified release area with a depth-averaged quasi-three-dimensional model of Voellmy-type. A number of test runs in different climate zones of Norway showed a substantial improvement in accuracy over the existing maps. Avalanche experts tend to estimate the effect of forests on the release probability much more optimistically than the published theories implemented in NAKSIN, indicating the need for focused research. Mapping the hazard due to the suspension layer of dry-snow avalanches will require a new generation of numerical models. NAKSIN should be readily adaptable to other geographic and climatic conditions.

Anmerkning til leseren / ***Note to the reader***

This Technical Note—although released in 2020—derives from a manuscript written in early 2018 for inclusion in a topical issue of *Annals of Glaciology*, related to the IGS Symposium "Cryosphere and Biosphere" in Kyoto, Japan in March 2018, where this work was presented for the first time. Thus it reflects the state of development of NAKSIN at that time. However, the authors decided to withhold publication of the manuscript because NAKSIN was undergoing significant changes. This situation has persisted until at present, but the need for a comprehensive description of the approach and the program structure has been increasingly felt. For this reason, the original manuscript is made accessible in this Technical Note to bridge the time until an up-to-date description is published in a scientific journal.

Innhold / *Table of Contents*

Table of Contents

1 Introduction: Avalanche hazard indication maps

A prerequisite for dealing with snow avalanche hazard in a rational way is knowing how far avalanches (with a given occurrence probability) can reach. In many mountain regions, avalanche-safe areas are scarce, hence the hazard needs to be mapped with considerable precision; this is an expensive process, however. In Norway, *avalanche hazard indication maps* (AHIM in the following) delineate potentially endangered areas in a rather conservative way and can be used to guide land-use planning and to quickly determine whether a potential construction site requires more detailed hazard mapping or not. AHIMs have proved to be a very useful tool in Norway, and one may expect that they would be similarly useful in other avalanche-prone countries, particularly if the population density is low to moderate.

The first generation of AHIMs was produced manually between 1975 and 2007 for selected areas only, combining interpretation of maps and ortho-photos, rapid surveying and run-out calculations with the topographic-statistical α-β model (Bakkehøi and others, 1983) for critical avalanche paths. The second-generation AHIM (AHIM-2G in the following), issued in 2010, covers the entire country; it was produced—without expert intervention—from a digital elevation model (DEM) with 25 m spatial resolution (Derron and Sletten, 2016). Each cell with slope angle between 30° and 55° is considered a release area and is the starting point of a run-out calculation with a modified α-β model. This model finds the point with run-out angle $\alpha - 2.3°$ along the path of steepest descent and also includes all cells within a corridor of predefined opening angle to both sides of the steepest path. The main advantages of this map set are the complete coverage of Norway, the objectivity of the method, and the moderate cost compared to manual mapping. However, the following weaknesses were soon discovered: (i) The cone spreading from both sides of the centerline of the path often predicts enormous run-out areas from minuscule release areas. (ii) The single parameter set used for the α-β model does not account for different behavior of avalanches in maritime or continental climate. (iii) The effect of forest on both the release probability and the run-out distance is neglected. Where the first-generation maps are available, they have been found to be more realistic and reliable than the AHIM-2G and take precedence.

An improved, third generation of AHIMs was clearly desirable. In discussions between the Norwegian Directorate of Water Resources and Energy (NVE), who are the government entity responsible for overseeing mitigation of gravitational natural hazards, and the authors, the following general goals were elaborated:

- Forest and climate effects and the lateral extent of the run-out area were identified as the problems with the greatest potential for improving map quality.
- The new AHIMs will primarily show the area endangered by snow avalanches with a nominal return period of 1000 years (corresponding to the safety standard for single-family homes stipulated by Norwegian law).

- The new AHIMs will not be produced for all of Norway at once, but according to the need perceived by each municipality. Accordingly, the emphasis is on developing the methodology for producing maps for areas of typically 100–1000 km^2. A limited amount of user intervention will be possible, e.g. for taking known avalanche events or the effects of powder-snow avalanches into account.
- A DEM with 10 m grid resolution, which is available for all of Norway, shall be used, with the option of using higher-resolution DEMs where they are available.
- The method and the corresponding code should be modular to facilitate future improvements.
- The new code should adhere to open standards and build on open-source software.

Under these conditions, both a terrain-following mass-point model (Maeno and Nishimura, 1987) and a quasi-3D (depth-averaged) continuum model (Gruber and Bartelt, 2007) became viable alternatives to the α-β model. In view of the anticipated increase of computing power and positive experience with quasi-3D models, the latter approach was chosen.

These premises are implemented in a linear work-flow:

1. Select a sufficiently large area of interest (AoI) and produce the corresponding computational grid from the DTM.
2. Interpolate meso-scale climate data to the computational grid.
3. Determine the potential release areas (PRAs) from geometric criteria (slope, size, curvature, shape).
4. Estimate the release probability for each PRA, taking into account terrain, climate and forest cover.
5. Estimate the release depth and friction parameters of each avalanche in the computational domain.
6. Carry out numerical simulations with the quasi-3D model.
7. Combine the calculated avalanche areas from all paths and draw the AHIM.

Python 3 was chosen as the programming language for the framework and the modules of the work-flow—collectively called NAKSIN—, because most geographic information systems (GIS) offer a Python application programming interface. For the run-out calculation, MoT-Voellmy is used (see the next section); it is an ISO-C code that can easily be called from a Python routine. For the manipulation of geographic data, we use

functions from the Geospatial Data Abstraction Library (GDAL) (GDAL/OGR contributors, 2018), NumPy (Oliphant, 2006) and SciPy (Jones and others, 2001–) functions or wrote dedicated Python functions; a GIS is only needed to overlay the hazard areas on a background map and to apply the desired symbolization. Geographic input data (DEM, climatic and forest data) and NAKSIN's output—the hazard area—are raster files in the simple, published ESRI ASCII Grid or BinaryTerrain 1.3 formats. All parameter choices in a session are documented in ASCII format in the master set-up file.

The rest of the paper will describe some of the steps in the work-flow in more detail and present some examples that illustrate the improvement over AHIM-2G and the issues that require further research and development.

2 The run-out model

For the run-out calculations, the NAKSIN script calls MoT-Voellmy, a simple quasi-3D model developed at NGI. Very similar to the well-known code RAMMS (Christen and others, 2010), it solves the depth-averaged mass and momentum balance equations for an incompressible fluid:

$$\partial_t h + \boldsymbol{\nabla} \cdot (h\mathbf{u}) = w_e(h, \|\mathbf{u}\|), \tag{1}$$

$$\partial_t (h\mathbf{u}) + \boldsymbol{\nabla} \cdot (h\mathbf{u}\mathbf{u}) + \boldsymbol{\nabla}\left(g_\perp h^2/2\right) = h\mathbf{g}_\parallel + \hat{\boldsymbol{\tau}}_b \tag{2}$$

Here, h is the flow depth (measured perpendicular to the slope), $\mathbf{u}$ is the depth-averaged slope-parallel component of the velocity, $g_\perp > 0$ and $\mathbf{g}_\parallel$ are the slope-normal and slope-parallel components of the gravitational acceleration, g. The earth pressure is assumed hydrostatic, i.e., active and passive states are not distinguished. NAKSIN does not use the bed entrainment option that is available in MoT-Voellmy, setting $w_e \equiv 0$. Voellmy's (1955) friction law, extended for the dominant terrain curvature effects, is adopted for the bed shear stress per unit density, $\hat{\boldsymbol{\tau}}_b$ (a vector):

$$\hat{\boldsymbol{\tau}}_b = -\frac{\mathbf{u}}{\|\mathbf{u}\|}\left[\mu h(g\cos\theta + \kappa\mathbf{u}^2) + k\mathbf{u}^2\right], \tag{3}$$

κ is the terrain curvature in the flow direction. μ and k are the dimensionless coefficients of quasi-static friction and of "turbulent" drag, respectively; k relates to the traditional, dimensional Voellmy drag coefficient as $\xi = g/k$. μ and k may vary both in space and time. Von Neumann boundary conditions allow the avalanche to flow out of the domain. The initial conditions are $\mathbf{u} \equiv \mathbf{0}$ in the entire domain, $h(\mathbf{x}, 0) = h_0(\mathbf{x}) > 0$ in the release area and $h(\mathbf{x}, 0) = 0$ outside.

These equations are solved in a domain that follows the terrain surface and whose vertical projection is a rectangular array of quadratic cells. The numerical scheme is the simplest version of the Method of Transport (Fey and others, 1997), with only the principal wave corresponding to the flow velocity retained. Due to central differencing of the earth-pressure term, the code in its present version is somewhat prone to checkerboard

oscillations, but they do not usually affect the simulated run-out distances. For the time evolution, a first-order explicit scheme with adaptive time stepping is used.

The Voellmy model does not fully describe the dynamics of dry-snow avalanches so that the friction parameters must be tuned according to the size and assumed return period of the avalanche, the climatic conditions and the topographic characteristics of the path. The calibration developed by Gruber (1998) for the Swiss Alps was later refined for RAMMS in (Bartelt and others, 2017, ch. 7). It gives plausible run-out distances also in Norway if the altitude zones are adjusted for the high latitudes of Norway. As MoT-Voellmy and RAMMS produce very similar simulation results with identical initial data and friction parameter fields, this calibration was adopted for NAKSIN, but modified in two respects: (i) μ and k are interpolated linearly with respect to avalanche volume, temperature and terrain curvature, and logarithmically for avalanche frequency. (ii) Instead of three altitude zones with abrupt transitions at 1000 and 1500 m a.s.l., NAKSIN uses the average winter temperature (December to February) as a physically more immediate proxy for the processes determining friction through the snow properties. Climate normals from Switzerland (MeteoSwiss, 2018) show that $T_{\text{winter}}(1000\,\text{m a.s.l.}) \approx -2.0°\text{C}$ and $T_{\text{winter}}(1500\,\text{m a.s.l.}) \approx -4.0°\text{C}$ in the Swiss Alps. The friction values are interpolated linearly over the range $-5.0°\text{C} \leq T_{\text{winter}} \leq -1°\text{C}$ between the values for the lowest and highest altitude category in the RAMMS calibration.

3 Potential release areas

Whereas the AHIM-2G used only a simple slope-angle criterion to delineate potential release areas (PRAs), NAKSIN adds a sequence of further topographic or geometric conditions to it: A threshold on the convexity of contour lines (defaulting to $-0.05\,\text{m}^{-1}$) eliminates sharp ridges and shoulders, possibly dividing some PRAs. Next, a simple algorithm eliminating protrusions and "bottlenecks" is applied iteratively until no further eliminations occur; see Appendix A for details. Subsequently, small "islands" within a PRA are added to it even though their slope angles are outside the allowed range. Then, PRAs below a minimum size (user-selectable in the range 200–1000 m^2, default 400 m^2) are eliminated because the corresponding release probability would be too small. After this, connected patches are identified and numbered.

This algorithm produces plausible results in many cases. However, in some long glacial valleys with many tributaries and steep, smooth sides or in long, steep gullies, PRAs with unrealistic aspect ratio or size may arise. Excessively long PRAs are reduced starting from the stauchwall until their altitude range is within a user-set bound (defaulting to 400 m). PRAs whose area exceeds a user-set threshold (default 100,000 m^2) are split along the boundaries of watersheds.

4 Release probability without forest effects

An important step in the mapping process is to eliminate all release areas with a release probability below a certain threshold, set at $0.001\,\mathrm{y}^{-1}$ by default. There is presently no well-established method for determining the release probability in a given avalanche path, hence the method described here has to be considered preliminary. Except for the spatial interpolation of climate data (average winter air temperature, average maximum snow height and maximum snow fall within three days), it is a simplified version of the model proposed by Gauer (2018). We first consider the case without forest and include forest effects in the next section.

The climate data relevant for NAKSIN can be derived from the seNorge data set released by the Norwegian Meteorological Institute (met.no). seNorge is based on spatial interpolation of temperature and precipitation data from Norwegian weather stations, augmented with the output of physical or empirical models specific to each meteorological variable (Saloranta, 2012, 2016). The grid with a cell size of 1 km^2 covers the entire country with daily data from 1957 onward. Normal winter temperature and the extreme-value statistics of snow depth, $\mathrm{HS}_{\mathrm{max}}$, and snow precipitation within a three-days period, $\mathrm{HNW}_{\mathrm{3d}}$, are particularly interesting for our purposes. These data were extracted from the time series of the seNorge data set and, for each grid cell (m, n), fitted to generalized Pareto distributions with location 0 of the form

$$C_{Q,mn}(q) = 1 - \left(1 + \xi_{Q,mn}\frac{q}{\sigma_{Q,mn}}\right)^{-1/\xi_{Q,mn}}, \tag{4}$$

where $C_{Q,mn}$ is the (cumulative) probability of the variable Q taking values smaller or equal q in grid cell (m, n). $\sigma_{Q,mn}$ is the local scale factor, $\xi_{Q,mn}$ the local shape coefficient in that cell. The generalized Pareto distribution is a preliminary choice, subject to further analysis of the seNorge data set.

Even though the gridding performed by met.no is already fraught with considerable uncertainty, bold further downscaling to the resolution of the DEM (10 m) is needed because the variations of the climatic variables can be large within 1 km^2. For each climate variable Q, we determine the base value at sea level, q_0, and the lapse rate, r from a linear regression of the data Q_{mn} against the corresponding cell-average altitudes Z_{mn} in the mapping area. The value of Q in cell (i, j) of the high-resolution DEM is then estimated as $q_{ij} = q_0 + rz_{ij}$. This method is simple and works also in coastal areas where seNorge data for snow and precipitation may be missing in many cells of the rectangular mapping area. While Gauer (2018) disregards the relief within seNorge grid cells and interpolates bilinearly in the horizontal dimensions, we neglect here the horizontal gradients to estimate the vertical ones. More advanced interpolation methods like kriging should be explored in the future. Note, however, that the important effects of the local wind field cannot be recaptured by interpolation.

In order to include the main factors driving or opposing avalanche release in a sufficiently simple model, we follow Gauer (2018) and apply the infinite-slope approximation. The

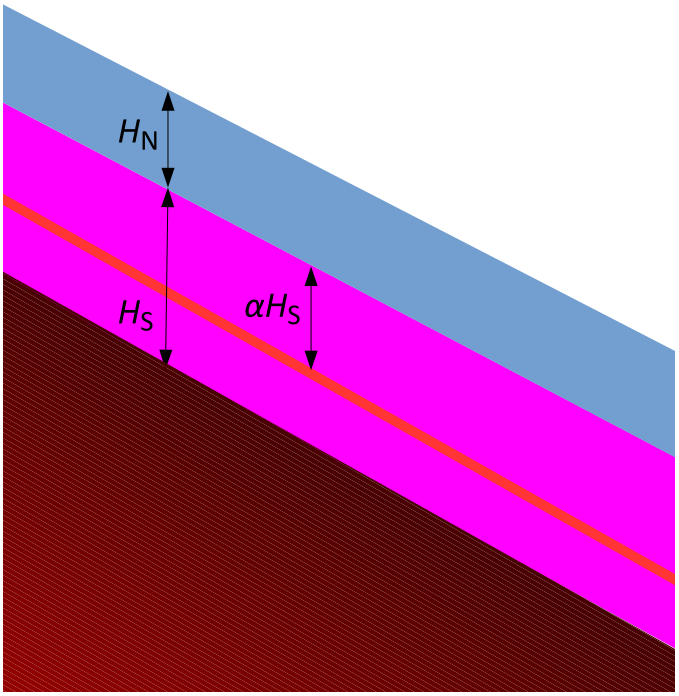

Figure 1 Simplified snowpack structure assumed for calculating release probability. H_S and H_N are old-snow depth and new-snow depth, respectively, and τ_w is the strength of the weak layer, which is represented by the thin red layer within the old snow.

snowpack is schematically depicted as shown in Fig. 1, with a weak layer of strength τ_w located a distance αH_S below the interface between the old and new snow, whose heights are H_S and H_N, respectively. Fracture is assumed to occur if the down-slope gravitational traction on the weak layer,

$$\Sigma = (\alpha H_S \rho_S + H_N \rho_N) g \sin\theta \cos\theta, \tag{5}$$

exceeds τ_w. ρ_S and ρ_N are the densities of the two layers. This simple stability criterion can be expressed in terms of a characteristic function,

$$\Theta(1 - \tau_w/T) = \begin{cases} 1, & \text{if } \tau_w < \Sigma \quad \text{(fracture)}, \\ 0, & \text{if } \tau_w > \Sigma \quad \text{(stability)}. \end{cases} \tag{6}$$

If H_N is large enough, fracture will occur before the end of the snowfall. The fracture depth (measured perpendicular to the slope) evaluates to

$$d_0 = \frac{\tau_w}{\rho_N g \sin\theta} - \left(\frac{\rho_S}{\rho_N} - 1\right) \alpha H_S \cos\theta. \tag{7}$$

We arrive at a probabilistic formulation of avalanche release by regarding the characteristic function (6) as a conditional release probability density for given values of the

independent stochastic variables H_S, H_N, τ_w and α. Suppose that the latter have probability distribution functions (PDFs) $\tilde{p}_1(H_N)$, $p_2(H_S)$, $p_3(\tau_w)$ and $p_4(\alpha)$. Henceforth, we denote absolute PDFs by p and PDFs per unit time interval by $\tilde{p}$. Then the release probability in PRA i is

$$\tilde{P}_{A,i} = \int_0^{H_{N,\max}} \int_0^{H_{S,\max}} \int_{\tau_{w,\min}}^{\tau_{w,\max}} \int_0^1 \Theta\left(1 - \frac{\tau_w}{\Sigma(H_N, H_S, \alpha)}\right) \times p_4(\alpha)\mathrm{d}\alpha\, p_3(\tau_w)\mathrm{d}\tau_w\, p_2(H_S)\mathrm{d}H_S\, \tilde{p}_1(H_N)\mathrm{d}H_N. \tag{8}$$

For given distributions of the stochastic variables, one can evaluate Eq. (8) using a Monte-Carlo approach. To obtain the distribution of the fracture depth, one needs to record the value of d_0 according to Eq. (7) for each trial that leads to release.

The snow densities ρ_S and ρ_N should be considered stochastic variables, but at this stage we presume their variability to be included in the probability distribution of H_S and H_N, respectively. Their values tend to increase with average winter temperature, $\bar{T}$; we capture this by choosing

$$\rho_S(\bar{T}) = \max[200.0,\ \min(400, 320 + \bar{T}/0.05°\mathrm{C})]\,\mathrm{kg\,m^{-3}};$$
$$\rho_N(\bar{T}) = 0.5\rho_S, \qquad \rho_w = 0.8\rho_S. \tag{9}$$

Snow strength increases approximately exponentially with density at constant temperature (e.g. Mellor, 1975). Mellor and Smith (1966) found a non-dimensional relation that describes their experiments on the temperature dependence of snow strength at constant density reasonably well. Assuming the mean winter temperature, $\bar{T}$, to be a sufficiently accurate proxy for the real temperature history, we arrive at

$$\tau_w(\rho_w, \bar{T}) \approx \tau_w(-10°\mathrm{C})\mathrm{e}^{\frac{\rho_w - 200\,\mathrm{kg\,m^{-3}}}{\rho_r}} \left(0.41 + 1.73 \cdot 10^{\frac{4.76°\mathrm{C}}{\bar{T}}}\right), \tag{10}$$

with $\rho_r \approx 50\,\mathrm{kg\,m^{-3}}$ inferred from (Mellor, 1975, Fig. 18).

The simplest choice for the distribution function of α is $p_4(\alpha) = 1$. Alternatively, one might weight $\alpha = 0$ and $\alpha = 1$ more strongly to account for surface hoar and depth hoar, respectively, using $p_4(\alpha) = a\delta(\alpha) + b\delta(1-\alpha) + 1 - a - b$, with $0 < a, b, a+b < 1$. For the weak-layer shear strength, which takes only positive values, a log-normal distribution seems appropriate:

$$p_3(\tau_w) = \frac{1}{\sigma\sqrt{2\pi}} \frac{1}{\tau_w} \exp\left[-\frac{(\ln(\tau_w/\tau_r) - \mu_3)^2}{2\sigma^2}\right] \tag{11}$$

With $\sigma = 0.15$, the standard deviation is about 15% of the mean strength $\langle\tau_w\rangle = \tau_r \exp(\mu_3 + \sigma^2/2)$. Setting the arbitrary reference strength τ_r to 1 kPa, typical values of μ_3—determined from Eq. (10)—are in the range $[-1, 1]$.

The PDF of the old-snow depth, H_S, will eventually be extracted directly from daily seNorge data. Presently, we assume that, in the course of a winter, all snow heights between 0 and $\mathrm{HS}_{\max}$ have the same probability. The PDF of H_S is then obtained from that of the yearly maximum values $\mathrm{HS}_{\max}$ as

$$p_2(H_S) = \Delta t \int_{H_S}^{\infty} \frac{1}{h} \tilde{p}_{\mathrm{HS,max}}(h)\mathrm{d}h. \tag{12}$$

The factor $\Delta t = 1\,\mathrm{y}$ converts the annual PDF $\tilde{p}$ to a correctly normalized absolute PDF.

5 Incorporation of forest effects

In this section, we propose simple approximations for the reduction of the release probability and the increased flow resistance due to forest. For the time being, we assume that the avalanche does not destroy the forest, and we disregard the enhanced potential damage due to entrained tree debris. We also indicate how the necessary quantitative information about the forest properties can be extracted for Norway from existing forest data sets covering most of the country.

As a short-cut, in step 3 of the workflow we exclude all cells from PRAs with a wintertime crown coverage CC (expressed in per cent) exceeding a threshold that depends on the local slope angle θ:

$$\mathrm{CC}_{\mathrm{thr}} = 60\% + \frac{4\%}{3^\circ}(\theta - 30^\circ). \tag{13}$$

We account for the influence of a forest stand on the release probability of avalanches by adding an effective shear strength τ_f due to the supporting force from the trees to the weak-layer shear strength τ_w in Eq. (8). Measurements of the snow loads on pylons and avalanche defense structures have led to a semi-empirical formula (Haefeli, 1939; Margreth, 2007; Ancey and Bain, 2015) that we simplify slightly in this application by using average values for the creep and glide factors. At a total snow depth H, the supporting force from a single tree with diameter D in a slope inclined at the angle θ is approximated as

$$F_t \approx \rho_S g H^2 (0.8D + 1.2H) \sin(2\theta). \tag{14}$$

This formula needs to be adapted to the situation where the snowpack consists of two layers with different densities and the supporting force $F_t(z)$ above some intermediate horizon z inside the lower layer is sought. The derivation is given in Appendix B. The effective added shear strength is then

$$\tau_f = F_t(H_S, z, H_N, \rho_s, \rho_n, \bar{D}) n \cos\theta, \tag{15}$$

also with n the number of trees per unit (horizontal) area and $\bar{D}$ the average trunk diameter. The factor $\cos\theta$ converts n to the tree density per unit oblique area.

The modified equation can be evaluated in the same way as before since no new stochastic variables have been introduced. However, since the release probability may be strongly reduced by the forest, a larger number of Monte Carlo trials may be needed to attain sufficiently small statistical uncertainty.

To calculate the braking effect of a forest on the moving avalanche, we assume that the total force scales linearly with the number of trees. For super-critical flows—the dominant situation for snow avalanches—in dense forest, this is likely to underestimate the resistance (Tai and others, 2001). Averaged over a suitable area, the braking force exerted by the trees can be expressed as an extra contribution to the bed shear stress per unit mass, $\hat{\tau}_{\text{tree}}$, as

$$\hat{\boldsymbol{\tau}}_t = -\frac{\mathbf{u}}{\|\mathbf{u}\|} F_t^{(d)}(h, \|\mathbf{u}\|) n \cos\theta, \tag{16}$$

where $F_t^{(d)}$ is the force exerted by a single tree in a rapid flow. As discussed in Appendix B, the granular nature of avalanching snow leads to a velocity-independent contribution as well as to one proportional to the square of the flow velocity, which can be captured by modifying the friction coefficients of the Voellmy model by

$$\Delta\mu = 1.25\, nDh\cos\theta \quad \text{and} \quad \Delta k = 0.5\, nDh\cos\theta. \tag{17}$$

This is easily implemented in MoT-Voellmy, which allows for variable friction coefficients $\mu(\mathbf{x}, t)$ and $k(\mathbf{x}, t)$. For an avalanche with a flow depth of 1.5 m flowing through a moderately dense, mature forest with $n = 400\,\text{ha}^{-1}$ and $D = 0.4\,\text{m}$ with a slope angle of 30°, one finds $\Delta\mu = 0.03$ and $\Delta k = 0.012$. In many cases, $\Delta\mu$ and Δk will be smaller. For comparison, typical parameter ranges without forest are $0.15 < \mu < 0.3$ and $0.003 < k < 0.01$.

Data on stand density, n, and average tree diameter, D, is not directly available at present but must be extracted from other data. In Norway, the data sets SAT-SKOG and SR16 provide a number of parameters characterizing forest stands. Based on satellite images from 2006 and ground truth from a network of periodically visited study plots, SAT-SKOG covers all of continental Norway except the northernmost county Finnmark at a spatial resolution of about 30 m (Gjertsen and Nilsen, 2012). SR16 uses more recent high-resolution aerial LiDaR data instead of satellite data, but covers only about 25% of the country at present. See Appendix C for a brief summary of the relations that were used to extract the quantities of interest in NAKSIN.

6 Preliminary test results

Testing NAKSIN in a completely objective way is impossible because the true hazard-zone boundaries will never be known. As the best available approximation, we used areas where detailed avalanche hazard mapping, including extensive field work, has been carried out recently. We chose locations at different latitudes, in maritime and continental climate, above timberline and in densely forested terrain, and with a wide variety of terrain features. Below we present two cases that show the potential of the new method.

Similar results with realistic hazard zones were obtained in all other test sites with maritime climate, except in locations where (large) avalanches are known to produce damaging powder-snow clouds. In those cases, the experts who produced the detailed hazard maps enlarged the hazardous areas obtained by numerical simulation according to the available damage records.

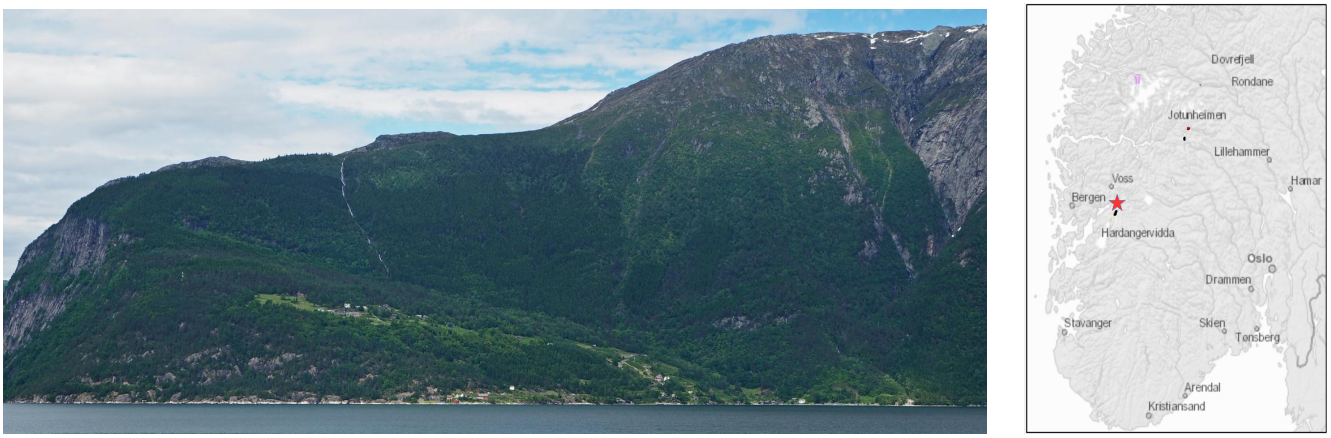

Figure 2 View of the the Tjoflotviki area from south across the Hardanger Fjord (left) and location map (right)

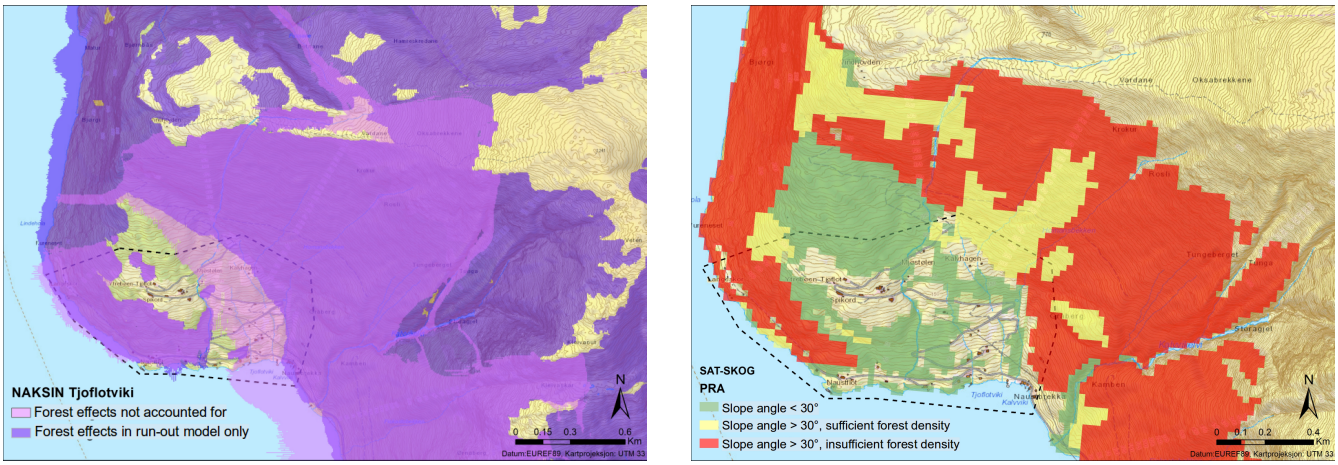

Figure 3 Left: *Endangered areas at Tjoflotviki according to NAKSIN simulations for all potential release areas with and without braking effect of forest taken into account.* Right: *Forested areas with sufficient stand density to prevent avalanche release according to NAKSIN criteria.*

Tjoflotviki in the municipality of Ullensvang, Hordaland County, is located deep inside the Hardanger Fjord, about 70 km east of Bergen and 100 km from the open sea (Fig. 2, right). Despite that distance and the proximity to large glaciers, the climate is rather maritime. The seNorge data set indicates annual mean temperatures in the range 4–6°C for the settlement areas near sea level and 0–4°C for the potential release areas.

Figure 4 Left: *Aerial photo of the Tyinstølen avalanche in January 2008, seen from the north. Photo courtesy of iBa80 Helge Frækaland, Natl. Public Road Administration.* Right: *location map.*

The corresponding ranges of annual mean precipitation are 3–4000 mm and more than 4000 mm, respectively. The potential release areas extend from about 400 m a.s.l. to a ridge that rises from 550 m a.s.l. in the north to about 1000 m a.s.l. in the east. Medium-dense to dense forest (predominantly spruce) is present to approximately 500 m a.s.l., whereas much thinner birch stands are found up to 700 m a.s.l. (Fig. 2, left).

In AHIM-2G, the entire area is shown as potentially endangered by avalanches. In contrast, NAKSIN run *without* forest effects indicates that most of the settlement and agriculture area on the plateau at 100–200 m a.s.l. can be considered safe, even if the braking effect of forest is not taken into account (Fig. 3). When it is taken into account, NAKSIN also designates most of the settlements in the southeastern corner of the study area as safe from avalanches. Comparison of the map of forest areas with sufficient stand density to prevent avalanche release (Fig. 3, right panel) with the photo in Fig. 2 shows that the simple criteria implemented in NAKSIN give plausible results in this case. The farm on the plateau has been inhabited for several centuries, and no damage from avalanches has been recorded.

In January 2008, a dry-snow avalanche at Tyinstølen, Vang municipality, Oppland County with a drop height of only 150 m (Fig. 4) ran far into a cabin area. Its run-out angle of 14.5° is the lowest recorded in Norway so far and is more than five standard deviations below the prediction of the α-β model. Accordingly, the hazard zone in the AHIM-2G ends 300 m before the observed run-out. Photographs show that the avalanche was strongly fludized, but that the deposits were not due to the powder-snow cloud. NAKSIN is able to capture this event without further tuning (Fig. 5). Tests in other areas with continental climate yet significant precipitation yielded similar results.

It has been observed, however, that NAKSIN in some cases strongly underestimates the release probability of avalanches in very dry and cold areas. This is likely the compound effect of underestimated lapse rates for precipitation, overestimated weak-layer shear strength and the neglect of blowing snow and deserves particular attention in the further

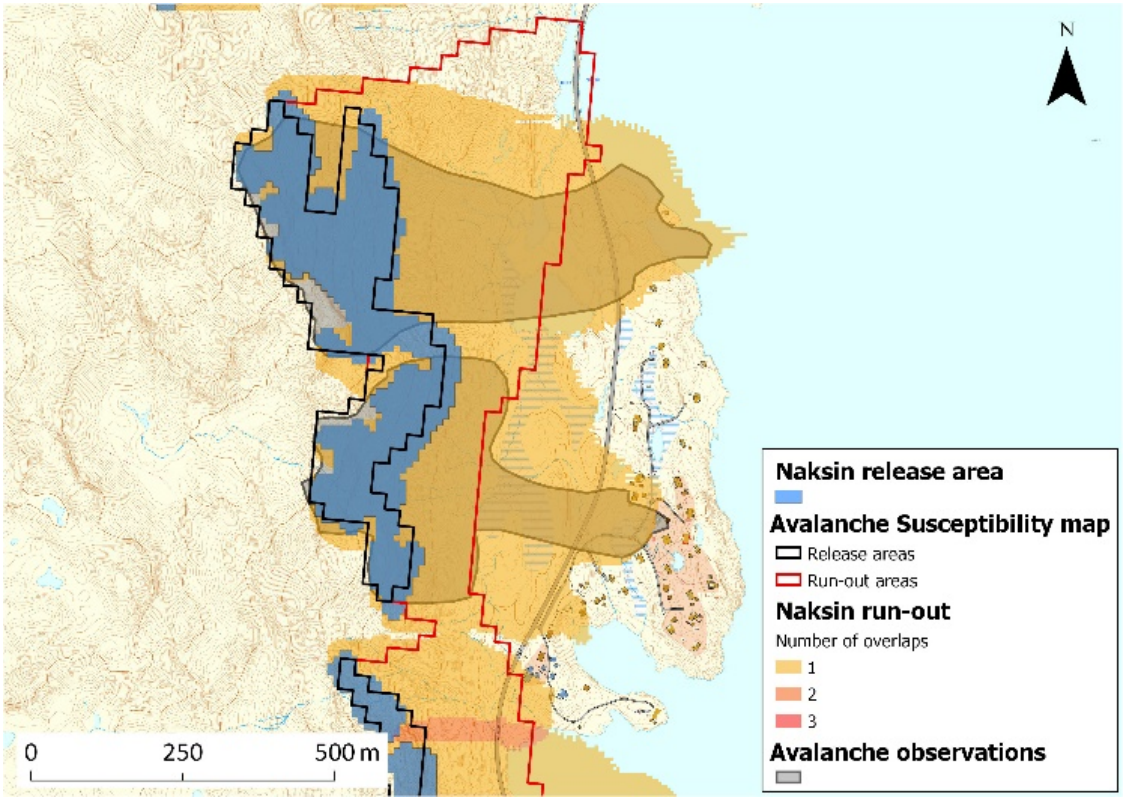

Figure 5 Comparison of avalanche release zones/hazard areas in the AHIM-2G (black/red lines) and from NAKSIN simulation (dark blue/yellow areas) with the events observed in 2008 (grey areas with dark outline).

development of the model.

7 Conclusions and outlook

The first tests of the mapping system NAKSIN have confirmed the viability of the chosen approach, and the improvements over the AHIM-2G are significant. In densely forested areas in maritime climate as well as in high-mountain areas with continental climate, a suitably calibrated dynamical model is far superior to the α-β model with a single calibration for all of Norway. The computation times are moderate even on today's standard hardware if the mapping area is not too large.

Some promising avenues for further development of NAKSIN are the following:

Size effects: Experience shows that the release area of an avalanche most often comprises only a fraction of the potential release area, this fraction increasing with the return period of the event (Maggioni and Gruber, 2003). Including this effect will be decisive for the quality of AHIMs from NAKSIN for return periods

less than about 300–1000 years. To this end, the infinite-slope approximation must be abandoned or at least refined by accounting for local variations of the slope angle within a PRA and for the resistive forces along the slab boundary, which are proportional to the length of the perimeter rather than the area of the slab.

Climate effects: An improved parameterization of the effects of temperature, wind and radiation on the PDF of τ_w is expected to improve NAKSIN's predictions considerably. Furthermore, alternatives to the presently assumed Generalized Pareto distribution for both H_S and H_N should be tested, e.g., a Gumbel distribution for H_S and a Generalized Extreme Value distribution for H_N. For large study areas, longitudinal gradients of the climate variables Q_{mn} ought to be accounted for; this could be done by computing base values $q_{0,mn}$ and lapse rates r_{mn} only from the cells within a limited distance from cell (m, n).

Further forest effects: Besides the direct mechanical resistance due to tree trunks, forests influence snow metamorphosis and weak-layer formation in a complex way through snow interception by the crowns, higher temperature, and reduced short-wave radiation and wind speeds (e.g. Gubler and Rychetnik, 1991). Such effects could be included in NAKSIN by modifying the PDFs of snowfall ($\tilde{p}_1$, p_s) and weak-layer shear strength (p_3) as a function of crown coverage (Gauer, 2016).

Wind effects: Blowing snow strongly influences both the release probability and the fracture height through the old-snow depth H_S, the snowfall height H_N, and the weak-layer shear strength τ_w. One may try to account for it by computing a simple topographic sheltering index $S_{ij}(\mathrm{DD}_k)$, like the one proposed by Winstral and others (2002), for each cell (i, j)) and for winds from different sectors DD_k, assigning weights to these sectors from regional statistics of geostrophic wind directions. Based on these index values and weights, the PDFs $\tilde{p}_1$, p_2 and p_3 would then be modified.

Run-out modeling: It would be appealing to replace the Voellmy model by a more physically realistic model and to reduce the role of friction-parameter calibration. However, with regard to the quality of the AHIMs, most could be gained by including the suspension layer ("powder-snow cloud") in the modeling because it may cause damage well beyond the run-out of the dense part in large avalanches.

Improved probability calculation: The Monte Carlo method for evaluating Eq. (8) is inherently inefficient if the release probability is low. Different approximation techniques like FORM or SORM (First-/Second-Order Reliability Method, Hasofer and Lind, 1974) should be explored to improve the performance of the code. One may also analytically calculate, for given H_S, z and τ_w, the minimum value of H_N needed for release and use its exceedance probability to reduce the number of integration variables in Eq. (8) by one.

Acknowledgements

The R&D work leading to this paper was financed by the Norwegian Water Resources and Energy Directorate (NVE) through the project 20150457 *Nye aktsomhetskart for snøskred i Norge*. Partial support for writing the paper came from NGI's general research grant from the Research Council of Norway. Peter Gauer, Katrine Mo, Marte Flaate Busengdal and Frode Sandersen contributed at different stages of the project. The authors are grateful to Odd Are Jensen for his constructive criticism.

References

Ancey C and Bain V (2015) Dynamics of glide avalanches and snow gliding. *Rev. Geophys.*, **53**(3), 745–784 (doi: 10.1002/2015RG000491)

Bakkehøi S, Domaas U and Lied K (1983) Calculation of snow avalanche runout distance. *Ann. Glaciol.*, **4**, 24–29 (doi: 10.3189/S0260305500005188)

Bartelt P, Bühler Y, Christen M, Deubelbeiss Y, Salz M, Schneider M and Schumacher L (2017) *RAMMS::AVALANCHE User Manual*. Version 1.7.0

Chehata D, Zenit R and Wassgren CR (2003) Dense granular flow around an immersed cylinder. *Phys. Fluids*, **15**(6), 1522–1531 (doi: 10.1063/1.1571826)

Christen M, Kowalski J and Bartelt P (2010) RAMMS: Numerical simulation of dense snow avalanches in three-dimensional terrain. *Cold Regions Sci. Technol.*, **63**(1–2), 1–14 (doi: 10.1016/j.coldregions.2010.04.005)

Derron MH and Sletten K (2016) Method for the susceptibility mapping of snow avalanches in Norway, Technical Report. NGU Report 2016.032, Geological Survey of Norway (NGU) and Institute of Geomatics and Risk Analysis (IGAR), University of Lausanne, Lausanne, Switzerland, revised edition

Fey M, Jeltsch R, Maurer J and Morel AT (1997) The method of transport for nonlinear systems of hyperbolic conservation laws in several space dimensions. Technical Report 97, Seminary for Applied Mathematics, ETH Zurich, Zürich, Switzerland

Gauer P (2016) Forest cover within Nye aktsomhetskart snøskred i Norge (NAKSIN). NGI Technical Note 20150457-04-TN, Norges Geotekniske Institutt, Oslo, Norway

Gauer P (2018) Avalanche probability: slab release and the effect of forest cover. In *Proceedings of the Intl. Snow Science Workshop Innsbruck 2018*, 76–83, International Snow Science Workshop

GDAL/OGR contributors (2018) *GDAL/OGR Geospatial Data Abstraction Software Library*. Open Source Geospatial Foundation

Gjertsen AK and Nilsen JE (2012) SAT-SKOG . Et skogkart basert på tolking av satellittbilder. Rapport fra Skog og landskap 23/2012, Norsk institutt for skog og landskap, Ås, Norway

Gruber U (1998) *Der Einsatz numerischer Simulationsmethoden in der Lawinengefahrenkartierung. Möglichkeiten und Grenzen*. Ph.D. thesis, University of Zurich, Dept. of Geography, Zürich, Switzerland, in German

Gruber U and Bartelt P (2007) Snow avalanche hazard modelling of large areas using

shallow water numerical methods and GIS. *Env. Mod. & Sftw.*, **22**(10), 1472–1481 (doi: 10.1016/j.envsoft.2007.01.001)

Gubler H and Rychetnik J (1991) Effects of forests near timberline on avalanche formation. In H Bergmann, H Lang, W Frey, D Issler and B Salm (eds.), *Snow, Hydrology and Forests in High Alpine Areas (Proceedings of the Vienna Symposium, August 1991), IAHS Publ. no. 205*, 19–38, IAHS Press, Institute of Hydrology, Wallingford, Oxfordshire, UK

Haefeli R (1939) Schneemechanik mit Hinweisen auf die Erdbaumechanik. In H Bader, R Haefeli, E Bucher, J Neher, O Eckel and C Thams (eds.), *Der Schnee und seine Metamorphose*, number 3 in Beiträge zur Geologie der Schweiz, Geotechnische Serie, Hydrologie, chapter 2, Kümmerly & Frey, Bern, Switzerland

Hasofer AM and Lind NC (1974) An exact and invariant first order reliability format. *J. Eng. Mech. Div. (ASCE)*, **100**, 111–121

Jones E, Oliphant T, Peterson P and others (2001–) SciPy: Open source scientific tools for Python. [Online; accessed <today>]

Maeno N and Nishimura K (1987) Numerical computation of snow avalanche motion in a three-dimensional topography (in Japanese). *Low Temp. Sci.*, **A 46**, 99–110

Maggioni M and Gruber U (2003) The influence of topographic parameters on avalanche release dimension and frequency. *Cold Regions Sci. Technol.*, **37**, 407–419 (doi: 10.1016/S0165-232X(03)00080-6)

Margreth S (2007) Defense structures in avalanche starting zones. Technical guideline as an aid to enforcement. Environment in Practice no. 0704, Federal Office for the Environment and WSL Swiss Federal Institute for Snow and Avalanche Research SLF, Bern and Davos, Switzerland, 134 pp.

Mellor M (1975) A review of basic snow mechanics. In *Snow Mechanics (Proceedings of the Grindelwald Symposium April 1974), IAHS Publ. no. 114*, 251–291, IAHS Press, Institute of Hydrology, Wallingford, Oxfordshire, UK

Mellor M and Smith JH (1966) Strength studies on snow. In *International Symposium on Scientific Aspects of Snow and Ice Avalanches, 5–10 April 1965, Davos, Switzerland: Reports and Discussions*, 100–113, Intl. Association of Hydrological Sciences, IAHS Publication nr. 69

MeteoSwiss (2018) Normal values per measured parameter. https://www.meteoswiss.admin.ch/home/climate/swiss-climate-in-detail/climate-normals/normal-values-per-measured-parameter.html, last accessed on 2018-07-19

Mitchell A (1976) *A Field Guide to the Trees of Britain and Northern Europe*. HarperCollins Distribution Services, New York, N.Y.

Näslund M (1940) Kubering av stående träd. Tall, gran och björk i norra Sverige. *Medd. Stat. Skogsförsöksanstalt*, **32**(4)

Oliphant TE (2006) Guide to NumPy. OpenAccess

Tai YC, Gray JMNT, Hutter K and Noelle S (2001) Flow of dense avalanches past obstructions. *Ann. Glaciol.*, **32**, 281–284 (doi: 10.3189/172756401781819166)

Voellmy A (1955) Über die Zerstörungskraft von Lawinen. *Schweiz. Bauztg.*, **73**(12, 15, 17, 19), 159–165, 212–217, 246–249, 280–285

Wassgren CR, Cordova JA, Zenit R and Karion A (2003) Dilute granular flow around an immersed cylinder. *Phys. Fluids*, **15**(11) (doi: 10.1063/1.1608937)

Widlowski JL, Verstraete M, Pinty B and Gobron N (2003) Allometric relationships of selected European tree species. Parametrizations of tree architecture for the purpose of 3-D canopy reflectance models used in the interpretation of remote sensing data. Betula pubescens, Fagus sylvatica, Larix decidua, Picea abies, Pinus sylvestris. Technical Report EUR 20855 EN, EC Joint Research Centre, TP 440, Ispra, Italy

Winstral A, Elder K and Davis RE (2002) Spatial Snow Modeling of Wind-Redistributed Snow Using Terrain-Based Parameters. *J. Hydrometeorol.*, **3**, 524–538 (doi: 10.1175/1525-7541(2002)003<0524:SSMOWR>2.0.CO;2)

A Appendix A

This appendix provides additional details on the algorithms used for delimiting potential release areas (PRAs).

In order to eliminate unrealistic protrusions and "bottlenecks" in PRAs, we apply a simple algorithm counting the number of release-cell neighbors for each potential release cell: Neighboring cells sharing an edge contribute one point, those only sharing a corner, one half point. Cells with a score less than 2.5 are identified as protrusions and eliminated because the fracture line is unlikely to follow such a ragged line. Bottlenecks are defined as cells that have no neighbors in one or two coordinate directions, even though their neighbor score may be as high as 4; they are eliminated and the release area cut in two because it is unlikely that the fracture will propagate across such a narrow "bridge". These criteria are graphically represented in Fig. 6. They are applied iteratively until no further eliminations occur. Note, however, that this algorithm is meaningful only if the cell size is close to the relevant length scale for avalanche release, which experience indicates to be of the order of 10 m. If the DEM resolution differs greatly from this value, the release areas should be determined on a DEM resampled to 10 m cell size.

In glacial valleys with many tributaries and steep, smooth sides, continuous PRAs may arise that are up to tens of kilometers wide and where even avalanche experts will find it difficult to identify the most likely PRA boundaries. In such cases, we apply an upstream basin-delineation algorithm: First, local topographic minima are identified. For each of these cells, all upstream cells are assembled into a watershed with its unique number. Then the over-sized release areas are divided along the boundaries between watersheds. For a given avalanche return period, the size of the release area depends sensitively on many factors like slope, terrain roughness, local climate and wind exposure. Moreover, it increases with return period (Maggioni and Gruber, 2003). For this reason, the choice of the size threshold for applying the watershed-delineation algorithm is left to the user; it defaults to 100,000 m^2.

In long, steep slopes, the slope criterion for PRAs may be met over a large fraction of the entire path, but it is unlikely that the release will occur over this entire altitude range. One option for restricting the PRA to a more realistic range is to select the steepest part of

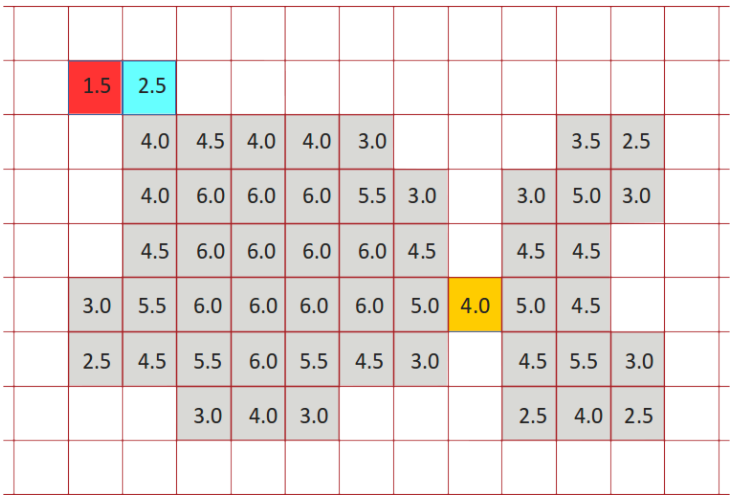

Figure 6 Graphical depiction of the algorithm for eliminating protrusions and bottlenecks from potential release areas (colored cells). The red cell is eliminated first, then the turquoise one because its neighbor count dropped to 2. The yellow cell is a "bottleneck" and is also eliminated.

the slope because the release probability increases with slope angle. However, we chose to focus on the uppermost part of the PRA, which tends to be widest and to receive most precipitation. Thus, the algorithm finds the highest elevation for each PRA and removes all cells whose elevation is less than that elevation minus a user-defined maximum elevation difference in the range 200–500 m. As this process may split some PRAs into two or more disconnected parts, each of which in addition may lie in more than one sub-basin, the splitting algorithm described above is applied once more.

B Appendix B

The semi-empirical formula (14) assumes a homogeneous snowpack and gives the total force on a tree. Modifying the formula for a layered snowpack and the force above a given horizon requires several assumptions, which ought to be based on a physical interpretation of Eq. (14). With the following two postulates, such an interpretation can be given and a modified formula derived: (i) One contribution to the force is due to creeping, and snow can be approximated as a Newtonian viscous fluid in this regard. (ii) The other contribution is due to the inherent shear strength of the snow, which behaves like a Coulomb material in this regard.

A simplified description of the force due to creep combines the velocity profile of stationary laminar flow on an incline,

$$u(y) = \frac{g \sin\theta}{\nu}(Hy\cos\theta - y^2/2), \tag{18}$$

with the force due to Stokes flow of undisturbed velocity U around a cylindrical obstacle

of diameter D,

$$\mathrm{d}F(U) = c\rho\nu U D \mathrm{d}y, \tag{19}$$

neglecting three-dimensional effects due to the free surface around the obstacle. The slope-normal coordinate, y, is related to the vertical one as $y = z\cos\theta$; ν is the kinematic viscosity of the fluid (units $\mathrm{m}^2\,\mathrm{s}^{-1}$). Note that the viscosity drops out if $u(y)$ from Eq. (18) is substituted for U in Eq. (19). The latter equation is to be integrated with density ρ_S in the interval $\alpha H_S \le z \le H_S$ and with density ρ_N over $H_S \le z \le H_S + H_N$.

Laboratory experiments on rapid, i.e., non-creeping granular flows, e.g. (Chehata and others, 2003), show that the force exerted by a single tree is proportional to its diameter, D, and the avalanche density, ρ_a. The drag of an obstacle in a flow is customarily written as $\bar{p}_{\mathrm{drag}} = (1/2)C_d(\mathrm{Re})\rho_a v^2$, with $C_d(\mathrm{Re})$ a dimensionless drag coefficient depending on the Reynolds number Re; v is the undisturbed flow velocity. In our case, we can set $v \approx \|\mathbf{u}\|$ since the Voellmy model implicitly assumes a uniform velocity profile and slip at the bed–flow interface. The standard definition of the Reynolds number for Newtonian fluids, $\mathrm{Re} = vD/(\rho_a\nu)$, needs to be modified for a granular fluid like snow, expressing it as the ratio of inertial forces and (visco-plastic) shear stresses, $\mathrm{Re} \sim \mathbf{u}^2/\hat{\tau}_b$. However, since the shear stress may be difficult to determine in a granular fluid because the shear strength may be only partially mobilized, we use the normal stress instead, as in, e.g., (Chehata and others, 2003). In a steady granular flow on an incline, the normal stress is proportional to the distance from the flow surface; we therefore take the average normal stress, $\sigma_n = (1/2)\rho g h\cos\theta$. Then the Reynolds number becomes

$$\mathrm{Re} \sim 2\mathrm{Fr}^2 = \mathcal{O}(1\text{–}200). \tag{20}$$

for typical avalanches in a forest. In this range, C_d varies very strongly with Re.

The experiments by Chehata and others (2003), covering dense flows in the range $10^{-4} < \mathrm{Fr} < 1$, found $C_d \propto \mathrm{Fr}^{-2}$ to high precision, the coefficient of proportionality being approximately 5. Numerical simulations of dilute flows at high Mach number and a wide range of Knudsen numbers (the ratio of the mean free path of the particles and the tree diameter in our case) reveal a more complex situation (Wassgren and others, 2003) that we need to simplify somewhat, keeping to the conservative side. We thus propose to use the relation

$$C_d(\mathrm{Fr}) \approx 1.0 + 5.0\,\mathrm{Fr}^{-2}, \tag{21}$$

which has the correct limit as $\mathrm{Fr} \to \infty$ for flows with Knudsen number $\mathrm{Kn} \ll 1$, which corresponds to relatively dense flows of small or moderately large particles. When multiplied with v^2 according to the drag formula, the second term in Eq. (21) contributes a velocity-independent friction, which dominates over the first term for $\mathrm{Fr} < 2$. In terms of the Voellmy model friction coefficients μ, k, Eq. (21) translates into

$$\Delta\mu = 1.25\,nDh\cos\theta \quad \text{and} \quad \Delta k = 0.5\,nDh\cos\theta. \tag{22}$$

The factor $\cos\theta$ converts from the number of trees per unit horizontal area to the number of trees per unit area on the slope inclined at an angle θ.

C Appendix C

Here we summarize how the product of stand density, n, and average tree diameter, D, can be extracted from the data sets SAT-SKOG (published in 2010) and SR16 (publication ongoing). The former is the result of automated interpretation of satellite images from Landsat-5 and Landsat-7 whereas the latter also makes use of orthophotos and LiDaR measurements. A comprehensive network of periodically visited study plots provide reference values for calibrating threshold values in the image analysis program (Gjertsen and Nilsen, 2012). Among the many quantities that are present with a spatial resolution of 30 m (16 m for SR16), the following are relevant for the present purpose: V, total timber volume per hectare; A, average age of the stand at the time of the satellite image; S, the prevailing species at the location; and Q, the quality (appraisal class) of the stand, expressed as the average height of the dominant species 40 years after these trees reached a height of about 1.3 m.

SAT-SKOG has important limitations: (i) It does not reflect the forest cover at a single point in time because the satellite images were obtained at different times. (ii) Many satellite images date back up to 20 years; since then, there have may have been significant changes in the forest cover, e.g. growth of forest on abandoned agricultural land or at higher altitudes, or radical timber harvesting. (iii) Errors may be large at the cell level. (iv) Estimating n and D from V, A, S and Q requires a number of assumptions that will introduce additional errors. The SR16 data set is of significantly better quality, but does not cover the entire country yet.

Gauer (2016) describes the assumptions and procedure for obtaining n and D from SAT-SKOG in detail. In Norway, the dominant tree species are birch (*betula*), pine (*pinus*) and spruce (*picea*); we will use indices B, P and S to distinguish between them where required. We use the the empirical correlations between tree height H and diameter $D_{1.3}$ at breast height (about 1.3 m) recommended by Widlowski and others (2003):

$$H_B(D_{1.3}) = 1.3\,\mathrm{m} + 32.1\,\mathrm{m}\exp(-16.36\,\mathrm{cm}/D_{1.3} - 10.76\,\mathrm{cm}^2/D_{1.3}^2), \quad (23)$$

$$H_S(D_{1.3}) = 1.3\,\mathrm{m} + 47.0\,\mathrm{m}\exp(-19.5\,\mathrm{cm}/D_{1.3}), \quad (24)$$

$$H_P(D_{1.3}) = 1.3\,\mathrm{m} + 50.5\,\mathrm{m}\exp(-24.88\,\mathrm{cm}/D_{1.3}). \quad (25)$$

According to Mitchell's (1976) approximation, the diameter at breast height increases linearly with tree age since reaching breast height, $A_{1.3}$,

$$D_{1.3}(S, Q, A_{1.3}) = f_g(S, Q)A_{1.3}, \quad (26)$$

with the growth factor f_g depending on tree species, S, and stand quality, Q. Given $Q(\mathbf{x})$ at location $\mathbf{x}$, the local value of f_g follows by solving Eqs. (23)–(25) with $H(D_{1.3})$ given by $Q(\mathbf{x})$ for $D_{1.3}$ and dividing by 40 years according to Eq. (26). $D_{1.3}$ is a reasonable approximation for the trunk diameter D in Eq. (22).

In order to find the stand density $n(\mathbf{x})$, we use the well-known empirical relation between

Table 1 Coefficients used in Näslund's (1940) parameterization of tree volume

Species	c_1 (m)	c_2 (—)	c_3 (—)	c_4 (m)
Birch	0.03715	0.02892	0.004983	0
Spruce	0.1202	0.01504	0.02341	−0.0659
Pine	0.09314	0.03069	0.002818	0

tree volume, height and breast-height diameter due to Näslund (1940):

$$v(S,H,D_{1.3}) = c_1(S)D_{1.3}^2 + c_2(S)D_{1.3}^2 H + c_3(S)D_{1.3}H^2 + c_4(S)H^2, \tag{27}$$

with the coefficients given in Table 1. The stand density can then immediately be estimated as

$$n(\mathbf{x}) = \frac{V(\mathbf{x})}{v(S(\mathbf{x}),H(S(\mathbf{x})),D_{1.3}(\mathbf{x}))}. \tag{28}$$

To speed up the calculations, Gauer (2016) developed approximations of the type

$$\frac{n}{n_{\text{ref}}} = 10^{b_{11}+b_{12}Q}\left(\frac{A_{1.3}}{A_{\text{ref}}}\right)^{b_{21}+b_{22}Q}\frac{v}{v_{\text{ref}}}, \tag{29}$$

$$\frac{nD}{(nD)_{\text{ref}}} = 10^{d_{11}+d_{12}Q}\left(\frac{A_{1.3}}{A_{\text{ref}}}\right)^{d_{21}+d_{22}Q}\frac{v}{v_{\text{ref}}}. \tag{30}$$

The coefficients are given in (Gauer, 2016); they depend weakly on the tree species and may be chosen equal until a more precise data set becomes available.

Kontroll- og referanseside / Review and reference page

Dokumentinformasjon/*Document information*		
Dokumenttittel/*Document title* Approaches to Including Climate and Forest Effects in Avalanche Hazard Indication Maps in Norway		**Dokumentnr./*Document no.*** 20150457-10-TN
Dokumenttype/*Type of document* Teknisk notat / *Technical note*	**Oppdragsgiver/*Client*** Norwegian Water Resources and Energy Directorate (NVE)	**Dato/*Date*** 2020-08-28
Rettigheter til dokumentet iht kontrakt/*Proprietary rights to the document according to contract* ÅPEN: Skal tilgjengeliggjøres i åpent arkiv (BRAGE) / *OPEN: To be published in open archives (BRAGE)*		**Rev.nr. & dato/*Rev.no. & date*** 0 / 2020-08-28
Emneord/*Keywords* Natural hazards, snow avalanches, hazard mapping, hazard indicaton maps, avalanche release probability, climate effects, forest effects		

Stedfesting/*Geographical information*	
Land, fylke/*Country* Norway	**Havområde/*Offshore area*** —
Kommune/*Municipality* —	**Feltnavn/*Field name*** —
Sted/*Location* —	**Sted/*Location*** —
Kartblad/*Map* —	**Felt, blokknr./*Field, Block No.*** —
UTM-koordinater/*UTM coordinates* **Sone:** 33N **Øst:** — **Nord:** —	**Koordinater/*Coordinates*** **Projeksjon, datum:** — **Øst:** ° ’ ” **Nord:** ° ’ ”

Dokumentkontroll/*Document control*
Kvalitetssikring i henhold til/*Quality assurance according to* NS-EN ISO9001

Rev.	**Revisjonsgrunnlag/*Reason for revision***	**Egenkontroll av/*Self review by:***	**Sidemanns-kontroll av/*Colleague review by:***	**Uavhengig kontroll av/*Independent review by:***	**Tverrfaglig kontroll av/*Interdisciplinary review by:***
0	Originaldokument	Dieter Issler 2020-08-27	Kjersti Gisnås 2020-08-28		

Dokument godkjent for utsendelse / *Document approved for release*	**Dato/*Date***	**Prosjektleder/*Project Manager***
	2020-08-28	Ulrik Domaas

NGI (Norges Geotekniske Institutt) er et internasjonalt ledende senter for forskning og rådgivning innen ingeniørrelaterte geofag. Vi tilbyr ekspertise om jord, berg og snø og deres påvirkning på miljøet, konstruksjoner og anlegg, og hvordan jord og berg kan benyttes som byggegrunn og byggemateriale.

Vi arbeider i følgende markeder: Offshore energi – Bygg, anlegg og samferdsel – Naturfare – Miljøteknologi.

NGI er en privat næringsdrivende stiftelse med kontor og laboratorier i Oslo, avdelingskontor i Trondheim og datterselskap i Houston, Texas, USA og i Perth, Western Australia.

www.ngi.no

NGI (Norwegian Geotechnical Institute) is a leading international centre for research and consulting within the geosciences. NGI develops optimum solutions for society and offers expertise on the behaviour of soil, rock and snow and their interaction with the natural and built environment.

NGI works within the following sectors: Offshore energy – Building, Construction and Transportation – Natural Hazards – Environmental Engineering.

NGI is a private foundation with office and laboratory in Oslo, branch office in Trondheim and daughter companies in Houston, Texas, USA and in Perth, Western Australia.

www.ngi.no

OSLO
TRONDHEIM
HOUSTON
PERTH

NORGES GEOTEKNISKE INSTITUTT
NGI.NO

Hovedkontor Oslo
PB. 3930 Ullevål Stadion
0806 Oslo

Avd. Trondheim
PB. 5687 Sluppen
7485 Trondheim

T 22 02 30 00
F 22 23 04 48
NGI@ngi.no

BANK
KONTO 5096 05 01281
ORG.NR. 958 254 318MVA

ISO 9001/14001
CERTIFIED BY BSI
FS 32989 / EMS 612006